

Dynamic Response Functions from Angle Resolved Photoemission Spectra

U. Chatterjee,^{1,2} D. K. Morr,¹ M. R. Norman,² M. Randeria,³ A. Kanigel,¹ M. Shi,^{1,4} E. Rossi,¹ A. Kaminski,⁵ H. M. Fretwell,⁵ S. Rosenkranz,² K. Kadowaki,⁶ and J. C. Campuzano^{1,2}

¹*Department of Physics, University of Illinois at Chicago, Chicago, IL 60607*

²*Materials Science Division, Argonne National Laboratory, Argonne, IL 60439*

³*Department of Physics, The Ohio State University, Columbus, OH 43210*

⁴*Swiss Light Source, Paul Scherrer Institut, CH-5232 Villigen, Switzerland*

⁵*Ames Laboratory and Department of Physics and Astronomy, Iowa State University, Ames, IA 50011*

⁶*Institute of Materials Science, University of Tsukuba, Ibaraki 305-3573, Japan*

(Dated: June 19, 2019)

We introduce a formalism for calculating dynamic response functions using experimental single particle Green's functions derived from angle resolved photoemission spectroscopy (ARPES). As an illustration of this procedure we estimate the dynamic spin response of the cuprate superconductor $\text{Bi}_2\text{Sr}_2\text{CaCu}_2\text{O}_{8+\delta}$. We find good agreement with superconducting state neutron data, in particular the (π, π) resonance with its unusual ‘reversed magnon’ dispersion. We anticipate our formalism will also be of useful in interpreting results from other spectroscopies, such as optical and Raman responses.

PACS numbers: 74.25.Jb, 74.25.Ha, 74.72.Hs, 79.60.Bm

The linear response to an external probe as a function of momentum and frequency is of great importance in elucidating the properties of complex materials. Examples include various two-particle correlation functions involving spin, current and charge probed by neutron, NMR, optics, and Raman spectroscopies. Recently there have also been major developments in the area of one-particle spectroscopies such as ARPES and scanning tunneling microscopy. The goal of this paper is to use one-particle spectroscopy data to gain insight into two-particle correlation functions. Specifically, we focus here on using the Green's functions obtained from superconducting state angle resolved photoemission spectroscopy (ARPES) [1] data in the high T_c cuprates to compute the dynamic spin susceptibility, which we then compare with inelastic neutron scattering (INS) [2].

From a theoretical point of view, dynamic response functions are difficult to calculate in general and many different approximate formalisms exist in the literature. For instance, there are two rather different approaches for computing the dynamic spin response for the high T_c cuprate superconductors. The first is based on the random phase approximation (RPA) [3] and related diagrammatic formulations [4]. This approach not only assumes momentum is a good quantum number, but also that the spin and charge degrees of freedom are coupled. The second is based on spin ladders separated by one-dimensional domain walls known as stripes. In this formalism spatial inhomogeneity is important, and the charge sector is assumed to be secondary when calculating the spin response [5]. Despite the quite different physics underlying these two schemes, the results for the calculated spin response function of the cuprates is similar, leading to one of the current dilemmas facing the

field of high T_c superconductivity.

It is thus important to go beyond a purely theoretical approach and directly employ information obtained from one experiment (ARPES), to make progress on interpreting the dynamic susceptibility measured by another (INS). We use a formalism based on a diagrammatic \mathbf{k} -space approach which goes beyond RPA in that it uses fully dressed Green's function obtained from ARPES data on $\text{Bi}_2\text{Sr}_2\text{CaCu}_2\text{O}_{8+\delta}$ (Bi2212), together with a near-neighbor exchange interaction. We compare the calculated superconducting state susceptibility with INS data. We obtain the (π, π) resonance seen in many cuprates [2], including Bi2212 [6], and also its unusual ‘reversed magnon’ dispersion as has been observed in $\text{YBa}_2\text{Cu}_3\text{O}_{7-\delta}$ (YBCO) [2].

We use ARPES spectra from a near-optimal sample ($T_c=90\text{K}$) of Bi2212, the data having been presented in earlier work [7, 8]. Bi2212 has physical properties which aid in our analysis [1]: its two-dimensional character greatly simplifies the interpretation of ARPES data, and it has a natural cleavage plane that acts to minimize the difference of the surface layer from the bulk. Although there does exist some INS data for the spin response on this material [6], it is not extensive due to the small size of Bi2212 single crystals. On the other hand, the data which do exist are quite similar to the much more extensive INS data for YBCO. Although there have been recent advances in ARPES for YBCO [9], the cleavage properties of this material are not as ideal as for Bi2212.

Quite generally, two-particle correlation functions can be written in terms of single-particle Green's functions and vertex parts [10]. Ignoring vertex corrections, the polarization bubble for the spin susceptibility in the superconducting state can be written as [11]

$$\chi_0(\mathbf{q}, \Omega) = \frac{1}{\pi^2} \sum_{\mathbf{k}} \int_{-\infty}^{\infty} d\nu d\epsilon [\text{Im}G(\mathbf{k}, \nu) \text{Im}G(\mathbf{k} + \mathbf{q}, \epsilon) + \text{Im}F(\mathbf{k}, \nu) \text{Im}F(\mathbf{k} + \mathbf{q}, \epsilon)] \frac{n_F(\nu) - n_F(\epsilon)}{\Omega + \nu - \epsilon + i\delta} = \chi_0^G + \chi_0^F \quad (1)$$

where Im denotes the Imaginary part of the normal and anomalous Green's functions G and F , and χ_0^G and χ_0^F denote the GG and FF contributions to χ_0 respectively.

We next describe in detail how $\text{Im}G$ is extracted from ARPES data and return later to the question of estimating the contribution of $\text{Im}F$ (which is not directly measured). ARPES probes the occupied part of the spectral function leading to the intensity $I(\mathbf{k}, \omega) \propto n_F(\omega) \text{Im}G(\mathbf{k}, \omega)$, where $n_F(\omega)$ is the Fermi function [12]. In order to extract $\text{Im}G$ from raw data we need to address several issues including data normalization, background subtraction, removing the effects of Fermi function, and extending $\text{Im}G$ to $\omega > 0$.

Starting from raw data, we first subtract the constant signal at $\omega > 0$ (due to second order light). All the spectra are then normalized at a high binding energy (~ 300 meV). This minimizes the effect of the intensity variations arising from dipole matrix elements. Next an ‘unoccupied’ state spectrum at a k far from k_F is used as an energy-dependent background [13] which is then subtracted from the data of interest. (We have checked that our final results for χ are not qualitatively affected by background subtraction.) After this, we divide the data by a resolution [14] broadened Fermi function to obtain $\text{Im}G(\mathbf{k}, \omega)$ for $\omega < 0$.

The next step is to determine the unoccupied part of the spectral function, $\text{Im}G(\mathbf{k}, \omega)$ for $\omega > 0$, which cannot be obtained directly from ARPES data. We obtain this by invoking particle-hole symmetry with respect to the Fermi surface: \mathbf{k}_F , $\text{Im}G(\mathbf{k}_F + \mathbf{k}, \omega) = \text{Im}G(\mathbf{k}_F - \mathbf{k}, -\omega)$, where \mathbf{k} is directed along the normal to the Fermi surface. This assumption should be reasonable in the superconducting state of optimally doped cuprates over an energy range in excess of the gap, as evidenced by the approximate particle-hole symmetry seen in tunneling experiments [15]. We have also checked that this assumption does not qualitatively affect our final results for χ_0 (by using $\text{Im}G$ with p-h asymmetry put in by hand).

Now we may use the $\text{Im}G$ derived from ARPES to calculate χ_0^G (we will discuss χ_0^F later). We limit the energy integration range in Eq. (1) to states which make the largest contribution which are within ± 150 meV of the chemical potential. As a check, we have also carried out an analysis with a larger integration range of ± 250 meV, but found no significant differences. Finally, to perform the \mathbf{k} -sum in Eq. (1), the ARPES data are interpolated to a regular grid and then reflected using square lattice group operations to fill the first Brillouin zone [8]. We used a 200×200 grid, but found no significant differences

for grid sizes ranging from 100×100 to 400×400 .

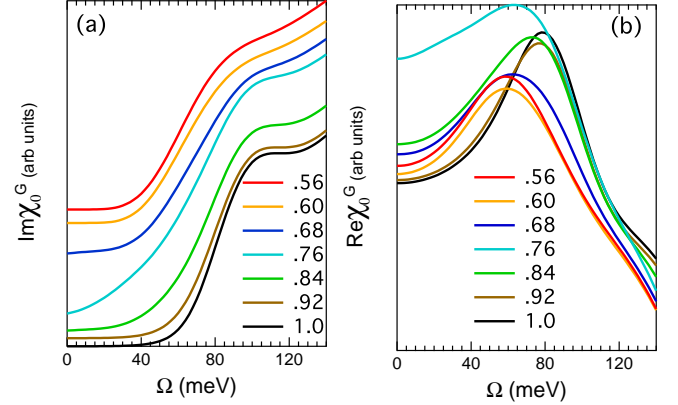


FIG. 1: (a) $\text{Im}\chi_0^G$ and (b) $\text{Re}\chi_0^G$ in the superconducting state as a function of frequency for momenta along $\mathbf{q} = \eta(\pi, \pi)$. The various curves, labeled by η , are offset for clarity in panel (a), noting that $\text{Im}\chi_0^G = 0$ at $\Omega = 0$.

Fig. 1(a) shows the calculated $\text{Im}\chi_0^G$ at $T=40$ K (superconducting state) as a function of the momentum transfer \mathbf{q} along the zone diagonal. We note that $\text{Im}\chi_0^G$ is greatly suppressed at low energies due to the gap to particle-hole (p-h) excitations in the superconducting state. The p-h gap is in general given by the sum of the superconducting gaps at two points on the Fermi surface separated by the wavevector \mathbf{q} . At $\mathbf{Q} = (\pi, \pi)$ we see in Fig. 1(a) a large gap whose midpoint is around 80 meV, roughly twice the maximum d-wave superconducting gap of $\simeq 40$ meV. The (π, π) vector connects the hot spots ($\epsilon_{\mathbf{k}} = \epsilon_{\mathbf{k}+\mathbf{Q}} = 0$) which are not too far from the zone boundary in Bi2212, and thus the hot-spot gap is comparable to the one at the antinode. We note that the threshold is quite broad (~ 40 meV) as a result of the intrinsic broadening of $\text{Im}G$ arising from self-energy effects in the data as well as resolution. As q decreases from Q , one sees the p-h gap decrease due to the d-wave anisotropy of the gap, and then disappear at $\mathbf{q}_n \simeq (0.76, 0.76)\pi$. \mathbf{q}_n is the wavevector corresponding to node-node scattering with the d-wave gap vanishing at the nodes. For $q < q_n$, the p-h gap increases again [3].

In Fig. 1(b) we show $\text{Re}\chi_0^G$ obtained from Eq. (1) [16]. First concentrating on \mathbf{Q} , we note the presence of a peak that corresponds to the gap midpoint of Fig. 1(a) as expected from Kramers-Kronig relations. This peak is broadest for \mathbf{q}_n where the p-h gap vanishes in the imaginary part.

We now turn to χ_0^F . Since $\text{Im}F$ is not available from experiment, we estimate the FF term as follows. We calculate the BCS $\chi_{0,\text{BCS}}^G$ and $\chi_{0,\text{BCS}}^F$ from Eq. (1) using the bare BCS Green's functions $G_0(\mathbf{k}, \omega) = (\omega + \epsilon_{\mathbf{k}})/(\omega^2 - \epsilon_{\mathbf{k}}^2 - \Delta_{\mathbf{k}}^2)$ and $F_0(\mathbf{k}, \omega) = \Delta_{\mathbf{k}}/(\omega^2 - \epsilon_{\mathbf{k}}^2 - \Delta_{\mathbf{k}}^2)$ with the experimentally measured dispersion [17] $\epsilon_{\mathbf{k}}$ and the measured $\Delta_{\mathbf{k}}$, which we find to be proportional to $(\cos k_x - \cos k_y)$ for this sample. We define the ratio of the real and imaginary parts, given by $\alpha_R(\mathbf{q}, \Omega) = \text{Re}\chi_{0,\text{BCS}}^F/\text{Re}\chi_{0,\text{BCS}}^G$ and similarly for $\alpha_I(\mathbf{q}, \Omega)$. We then assume that the missing contribution χ_0^F may be accounted for by $\text{Re}\chi_0 = \text{Re}\chi_0^G + \text{Re}\chi_0^F \simeq (1 + \alpha_R)\text{Re}\chi_0^G$ and $\text{Im}\chi_0 = \text{Im}\chi_0^G + \text{Im}\chi_0^F \simeq (1 + \alpha_I)\text{Im}\chi_0^G$. We will discuss below the extent to which our final results are affected by this approximation.

In order to carry out comparisons with INS data, or other probes such as NMR, the full spin susceptibility χ is needed. The most common approximation is to use the RPA form [3]

$$\chi(\mathbf{q}, \Omega) = \frac{\chi_0(\mathbf{q}, \Omega)}{1 - J(\mathbf{q})\chi_0(\mathbf{q}, \Omega)} \quad (2)$$

where we take the effective interaction to be $J(\mathbf{q}) = -J(\cos q_x + \cos q_y)/2$ corresponding to superexchange between near neighbor copper sites.

The polarization bubble presented in Fig. 1 is similar to that obtained from BCS theory [3] especially at low energies where the incoherent spectral weight in the ARPES data is small. Within BCS theory, which uses bare Green's functions, one has a true gap in the $\text{Im}\chi_0$ at \mathbf{Q} and a corresponding log divergence in the $\text{Re}\chi_0$. These features still persist in Fig. 1 albeit broadened by self-energy (and resolution) effects. As such, for some frequency smaller than the gap, one will obtain a pole in χ when $1 - J(\mathbf{q})\text{Re}\chi_0(\mathbf{q}, \Omega) = 0$ provided $\text{Im}\chi_0$ is very small (no damping) at the frequency of interest. This pole represents a collective mode, known as the spin resonance at \mathbf{Q} , which is prominently observed in INS data for YBCO [2] and Bi2212 [6]. Following this logic, we fix J by fitting the energy (42 meV) of the INS spin resonance at \mathbf{Q} for optimal doped Bi2212 [6]. Given the arbitrary normalization of the ARPES spectra, we cannot estimate χ_0 and therefore J in absolute units.

Fig. 2 shows the imaginary part of the full susceptibility χ as calculated from ARPES data as discussed above. In Fig. 3(a) we also present an intensity plot of $\text{Im}\chi(\mathbf{q}, \Omega)$ as a function of $\mathbf{q} = \eta(\pi, \pi)$ and Ω . From these two figures, we see there is a very sharp resonance peak at \mathbf{Q} , and as one moves away from \mathbf{Q} , the collective mode disperses, broadens in frequency, and loses intensity. Initially the mode disperses towards lower Ω , reaching a minimum at the node-to-node scattering vector \mathbf{q}_n . For $q < q_n$ the mode, which is now very broad and weak, disperses upwards. These dispersive features at incommensurate wavevectors are qualitatively similar to INS data for YBCO [2].

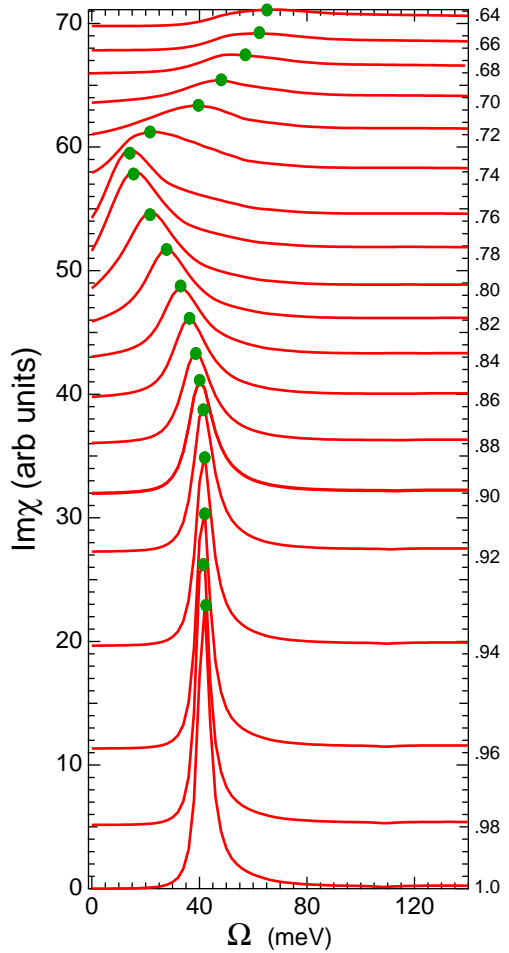


FIG. 2: $\text{Im}\chi$ as a function of frequency for several momenta $\mathbf{q} = \eta(\pi, \pi)$. The curves, labeled by η (shown on the right), are offset for clarity.

We now test our approximation for χ_0^F by setting $\alpha_R = \alpha_I = 0$, rescaling J to maintain the same resonance energy at \mathbf{Q} . The resulting dispersion which only includes the GG contribution is plotted in Fig. 3(b) (curve labeled G). Only minor differences are seen between this curve and the full calculation which includes both GG and FF contributions, labeled G & F in Fig. 3(b). This lack of sensitivity of the dispersion to the inclusion of FF terms is a consequence of the d-wave symmetry of the superconducting order parameter where χ_0^G and χ_0^F reinforce one another, i.e., α_R and α_I are both positive, near the (π, π) resonance. (In contrast, for an s-wave superconductor, χ_0^G and χ_0^F are opposite in sign, and there is no spin resonance.)

Comparing our results with the INS data and earlier RPA calculations, we arrive at the following conclusions. First, the self-energy effects present in the ARPES-derived Green's function do not affect low-energy physics such as the existence and sharpness of the (π, π) reso-

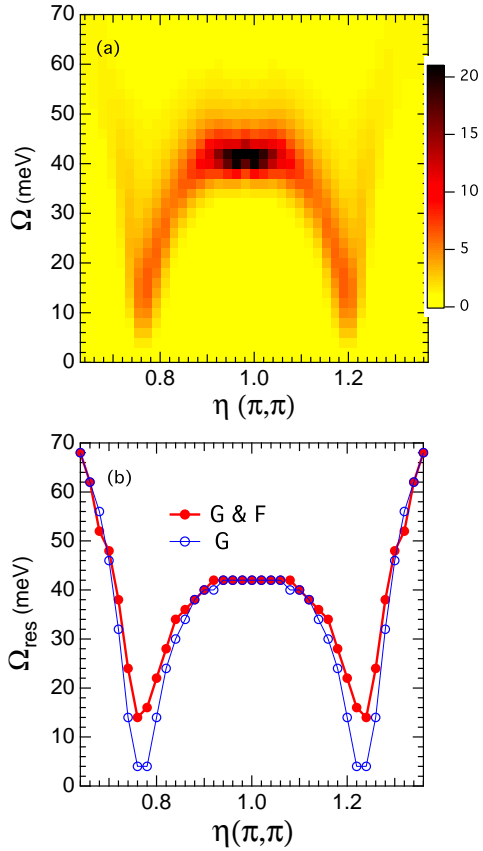


FIG. 3: (a) Intensity of $\text{Im } \chi(\mathbf{q}, \Omega)$ plotted in the $\mathbf{q} = \eta(\pi, \pi), \Omega$ plane. (b) Energy of resonance peak as a function of η along $\mathbf{q} = \eta(\pi, \pi)$. The curve labeled G & F includes both the GG and FF contributions and corresponds to the dispersion of the maximum intensity in panel (a). For comparison, we also show the curve labeled G which does not include the FF contribution; see text.

nance, or the mode dispersion. Second, vertex corrections do not play a major role in the spin channel. Note, however, that because of the arbitrary normalization of ARPES data, a constant (frequency independent) vertex correction cannot be elucidated. Finally, our results provide strong evidence for the interpretation of the resonance peak as a spin exciton [3].

To summarize, we compute the polarization bubble χ_0 using experimental Green's functions derived from ARPES spectra, and the full dynamic spin response obtained from a diagrammatic formalism assuming a near neighbor exchange interaction. Although this analysis requires several approximations, we find surprisingly good agreement with inelastic neutron scattering data for high temperature cuprate superconductors. Our results demonstrate a close relation between experiments probing the spin and single-particle excitations. Our formal-

ism is quite general, and can be used as well to compute other response functions, such as the current-current response function measured by conductivity.

This work was supported by NSF DMR-0606255, NSF DMR-0513415 (D.K.M.) the U.S. DOE, Office of Science, under Contracts No. W-31-109-ENG-38 (ANL), W-7405-Eng-82 (Ames), and Grant No. DE-FG02-05ER46225 (D.K.M.). The Synchrotron Radiation Center is supported by NSF DMR-0084402. U.C. would like to thank R. Sensarma for helpful discussions.

- [1] A. Damascelli, Z. Hussain and Z.-X. Shen, Rev. Mod. Phys. **75**, 473 (2003); J. C. Campuzano, M. R. Norman and M. Randeria, in *The Physics of Superconductors*, Vol. 2, ed. K. H. Bennemann and J. B. Ketterson (Springer, Berlin, 2004), p. 167.
- [2] J. Rossat-Mignod *et al.*, Physica C **185**, 86 (1991); H. F. Fong *et al.*, Phys. Rev. Lett. **75**, 316 (1995); M. Arai *et al.*, Phys. Rev. Lett. **83**, 608 (1999); P. Dai *et al.*, Phys. Rev. B **63**, 054525 (2001); S. Pailhes *et al.*, Phys. Rev. Lett. **93**, 167001 (2004).
- [3] J. Brinckmann and P. A. Lee, Phys. Rev. Lett. **82**, 2915 (1999); Y.-J. Kao, Q. Si and K. Levin, Phys. Rev. B **61**, 11898 (2000); M. R. Norman, Phys. Rev. B **61**, 14751 (2000) and **63**, 092509 (2001); F. Onufrieva and P. Pfeuty, Phys. Rev. B **65**, 054515 (2002); I. Eremin *et al.*, Phys. Rev. Lett. **94**, 147001 (2005).
- [4] See, e.g., C.-H. Pao and N. E. Bickers, Phys. Rev. B **51**, 16310 (1994); E. Demler and S.-C. Zhang, Phys. Rev. Lett. **74**, 4126 (1995); N. Bulut and D. Scalapino, Phys. Rev. B **53**, 5149 (1996).
- [5] M. Vojta and T. Ulbricht, Phys. Rev. Lett. **93**, 127002 (2004); G. S. Uhrig, K. P. Schmidt and M. Grunninger, Phys. Rev. Lett. **93**, 267003 (2004); C. D. Batista, G. Ortiz and A. V. Balatsky, Phys. Rev. B **64**, 172508 (2001).
- [6] H. F. Fong *et al.*, Nature **398**, 588 (1999).
- [7] A. Kaminski *et al.*, Phys. Rev. Lett. **86**, 1070 (2001).
- [8] U. Chatterjee *et al.*, Phys. Rev. Lett. **96**, 107006 (2006).
- [9] D. H. Lu *et al.*, Phys. Rev. Lett. **86**, 4370 (2001); S. V. Borisenko *et al.*, Phys. Rev. Lett. **96**, 117004 (2006).
- [10] G. D. Mahan, *Many-Particle Physics* (Plenum, New York, 1990).
- [11] J. R. Schrieffer, *Theory of Superconductivity* (Benjamin Cummings, Reading, MA, 1964).
- [12] M. Randeria *et al.*, Phys. Rev. Lett. **74**, 4951 (1995).
- [13] A. Kaminski *et al.*, Phys. Rev. B **69**, 212509 (2004).
- [14] ARPES data are also affected by finite energy and momentum resolutions which, in principle, can be deconvolved from the data but, in practice, have been found not to have a significant effect on $\text{Im } G$. See: M. R. Norman *et al.*, Phys. Rev. B **60**, 7585 (1999).
- [15] See, e.g., N. Miyakawa *et al.*, Phys. Rev. Lett. **83**, 1018 (1999); S. H. Pan *et al.*, Nature **413**, 282 (2001).
- [16] We take a finite $\delta = 0.5$ meV for the calculation of $\text{Re } \chi_0^G$.
- [17] M. R. Norman *et al.*, Phys. Rev. B **52**, 615 (1995).